Physical principles of the CircAdapt model

Maarten H.G. Heusinkveld *[1], Tammo Delhaas[1], Joost Lumens[1], Bart Spronck[2], Wouter Huberts[1], Alun D. Hughes[1], and Koen D. Reesink[1]

[1]CARIM School for Cardiovascular Diseases, Maastricht University, The Netherlands

[2]Department of Biomedical Engineering, Yale University, USA

*Address correspondence to M.H.G. Heusinkveld

Universiteitssingel 50, room 3.358, 6229 ER Maastricht

E-mail: m.heusinkveld@maastrichtuniversity.nl

Telephone: +31 43 388 1659

1 Introductory remarks

The CircAdapt model platform (www.circadapt.org) has a modular setup, consisting of a 0D whole-heart mechanics model, cardiac geometry adaptation model, valve hemodynamics model, and arterio-venous impedance model of the pulmonary and peripheral circulations. Given CircAdapt's cardiac and impedance modules have already been extensively described in various other works (1, 10, 12), we focus in this document on presenting its vascular module. Below, a complete description of the physical basis of our vascular module is presented as well as a benchmark test comparing simulated pressure and flow waves of the vascular module to those of a previously validated pulse wave propagation (PWP) model (8).

1.1 Vascular module

To model pressure and flow waves within segments of blood vessels, we assume 1) blood vessels to be longitudinally constraint, non-linear thick-walled elastic tubes, 2) blood to be incompressible and Newtonian and 3) that gravity forces can be neglected. Furthermore, we assume 4) no leakage of blood to small side-branches that are not explicitly modeled. Application of the laws of conservation of mass and momentum, and subsequent integration over the tube's cross-sectional area yield the governing equations (see e.g. Hughes and Lubliner (7)):

$$C\frac{\partial p}{\partial t} + \frac{\partial q}{\partial z} = 0 \ , \tag{1}$$

$$L\left(\frac{\partial q}{\partial t} + \frac{\partial}{\partial z}\int_A v_z^2 dA\right) + \frac{\partial p}{\partial z} = f \ , \tag{2}$$

where $p = p(z,t)$ is the pressure with z the axial vessel coordinate, and $q = q(z,t)$ flow rate. Furthermore, A denotes cross-sectional lumen area equivalent to πr_0^2, with r_0 reference lumen radius, and L and C are the tube inertance and compliance per unit length,

respectively. Term $L\frac{\partial}{\partial z}\int_A v_z^2 dA$ represents the convective acceleration term, with v_z the axial blood velocity. Term f represents friction force per unit volume caused by viscous properties of the blood, defined $f = 2\pi r_0 \tau_{\mathsf{w}}/A$ (3). Here, symbol τ_{w} denotes wall shear stress. After neglecting the convective acceleration term and assuming an approximate velocity profile to estimate τ_{w} (3), the governing equations can be rewritten to the telegrapher's equations:

$$-\frac{\partial q}{\partial z} = C\frac{\partial p}{\partial t}\,, \tag{3}$$

$$-\frac{\partial p}{\partial z} = L(\alpha_0)\frac{\partial q}{\partial t} + R(\alpha_0)q, \tag{4}$$

with $L(\alpha_0)$ and $R(\alpha_0)$ a characteristic Womersley number-dependent inertance- and resistance term, defined

$$L(\alpha_0) = g(\alpha_0)\,\frac{\rho}{A}\,, \tag{5}$$

$$R(\alpha_0) = h(\alpha_0)\,\frac{8\pi\eta}{A^2}\,, \text{with} \tag{6}$$

$$\alpha_0 = r_0\sqrt{\rho\omega_0/\eta}\,. \tag{7}$$

The functions $g(\alpha_0)$ and $h(\alpha_0)$ were derived by Bessems et al. (3) and depicted in Fig 1.

The characteristic Womersley number (α_0) describes the ratio of instationary inertia forces and viscous forces, governed by vessel radius (r_0), characteristic angular frequency ($\omega_0 = 2\pi/T$, with T the cardiac cycle duration), blood dynamic viscosity (η) and blood density (ρ), respectively. The rationale of this method is to calculate R and L based on the viscous boundary layer thickness, approximated by α_0 (3). To solve the governing equations, we also need a constitutive law to relate (changes in) transmural pressure

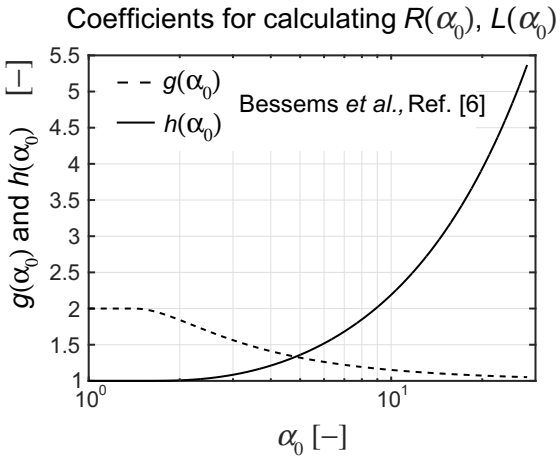

Figure 1: Coefficients g and h as a function of the characteristic Womersley number (α_0), used for calculating the characteristic Womersley number-dependent resistance $R(\alpha_0)$ and inertance $L(\alpha_0)$, respectively.

(p_{trans}) and (changes in) A. For this we chose a non-linear power-law given by

$$p_{\text{trans}}(A) = -p_{\text{ext}} + p_0 \left((1+b) \left(\frac{A}{A_0} \right)^{1+\frac{k/3-2}{1+b}} - \frac{bA_0}{A} \right) , \tag{8}$$

and

$$C = \frac{dA}{dp_{\text{trans}}} ,$$

with p_0 a reference pressure, A_0 a reference cross-sectional area, and k the vessel stiffness coefficient. Furthermore, b is a small fraction to avoid collapse of the tube with negative transmural pressure and p_{ext} represents a prescribed external pressure (if present). This type of constitutive law was chosen to phenomenologically capture the experimentally observed non-linear pressure-area relation of arteries and veins (2, 5). Now we can solve the resulting governing equations in either the time domain or frequency domain. In this study, we explicitly chose a time-domain approach, since this permits using non-linear boundary conditions as already present in the CircAdapt platform (12).

1.1.1 Solving strategy

Pressure and flow in a tube constitutes of the summation of a backward (bw) and a forward (fw) wave component (4). Therefore, at any location in the tube, it holds that

$$\begin{aligned} p(z,t) &= p_{\text{fw}}(z-ct) + p_{\text{bw}}(z+ct) \ , \\ q(z,t) &= \frac{p_{\text{fw}}(z-ct)}{Z} - \frac{p_{\text{bw}}(z+ct)}{Z} \ , \end{aligned} \tag{9}$$

with Z and c the characteristic Womersley number-dependent wave impedance and wave speed defined $Z = \sqrt{L(\alpha_0)/C}$ and $c = 1/\sqrt{L(\alpha_0)C}$, respectively (Appendix **??**). Considering the proximal inlet of a tube, we assume a linear relation between pressure $p_{\text{in}} = p(0,t)$ and flow $q_{\text{in}} = q(0,t)$, characterized by a zero-flow pressure p_{s} and an input resistance Z_{in}:

$$p_{\text{in}} = p_{\text{s}} + Z_{\text{in}} q_{\text{in}} \ . \tag{10}$$

The quantities p_{s} and Z_{in} can be calculated from p_{bw} and Z using the expressions given by

$$p_{\text{s}} = 2p_{\text{bw}} \ , \tag{11}$$

$$Z_{\text{in}} = Z \ . \tag{12}$$

The proximal load relates p_{in} to q_{in}. Using Eq. 10, p_{in} and q_{in} are calculated. Then, for further calculations we need to determine the amplitude of reflected wave p_{fw} at the entrance. It holds

$$p_{\text{fw}} = \frac{1}{2} p_{\text{s}} + Z q_{\text{in}} \ . \tag{13}$$

A tube, representing a blood vessel with length l, has a proximal and a distal side (Fig. 2). For each side Eqs. 9 to 13 may be applied with the remark, that flow at the distal side is directed outward, implying that the terms with flow $q_{\text{out}} = q(l,t)$ have to change

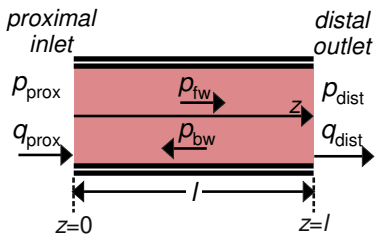

Figure 2: Overview wave propagation in a tube segment, directed along the z-axis. See text for description of symbols.

sign. At each moment in time, the amplitudes of the waves entering on both sides of the tube are calculated according to Eq. 13. This wave will arrive with a delay τ later at the opposite ending. As derived by Boucher and Kitsios (4) and applied by Krus et al. (9), the contribution of wave attenuation due to friction may be lumped at the proximal and distal side of the transmission line. Thus, for the proximal side it holds

$$p_{\text{bw,prox}} = p_{\text{bw,dist}}(t-\tau)\,\exp(-\zeta l),\ \text{with}\ \tau = \frac{l}{c}\,. \tag{14}$$

Symbols ζ and τ represent the attenuation constant and wave delay time, respectively. Attenuation constant ζ is assumed a function of the characteristic Womersley number:

$$\begin{aligned}\gamma = \zeta + j\beta &= j\omega\sqrt{L(\alpha_0)C}\sqrt{1-\frac{jR(\alpha_0)}{\omega L(\alpha_0)}} \\ \approx & j\omega\sqrt{L(\alpha_0)C}\left(1-\frac{jR(\alpha_0)}{2\omega L(\alpha_0)}+\mathcal{O}\left(\frac{1}{\omega^2}\right)\right) \\ \approx & \frac{R(\alpha_0)}{2\sqrt{L(\alpha_0)/C}}+j\omega\sqrt{L(\alpha_0)C}\,,\end{aligned} \tag{15}$$

with ζ the attenuation constant per unit length, β the phase constant per unit length and C the compliance per unit length.

Since $p_{\text{bw,dist}}$ is calculated before, and τ is assumed to be known, $p_{\text{bw,prox}}$ can be calculated. Pressure $p_{\text{fw,dist}}$ is to be calculated similarly. When knowing these wave amplitudes, zero-flow pressure p_{s} and an input resistance Z_{in} can be calculated on both sides of the

tube, using Eqs. 11 and 12 and their equivalents at the distal side. Pressures and flows, related to wave propagation may be superimposed on DC-components of flow q_{DC} and pressure p_{DC} (4). For small blood vessels, the Poiseuille resistance may become important. For the DC-pressure difference over the tube, related to q_{DC} it holds:

$$\Delta p_{\text{DC}} = q_{\text{DC}} \frac{8\pi\eta}{A^2} \ . \tag{16}$$

The DC-flow (q_{DC}), averaged over the tube length, changes due to contribution of flow waves entering and leaving from the proximal and distal side. In case no wave enters, the waves inside the tube will disappear completely after wave delay time τ. Using Eq. 18, reaching of the DC-steady state (i.e. term B of Eq. 17 becoming zero) was approximated by a first order differential equation with time constant equal to τ:

$$\frac{dq_{\text{DC}}}{dt} = \overbrace{\left(\frac{p_{\text{s,dist}} - p_{\text{s,prox}}}{2Z} - q_{\text{DC}} \right)}^{B} \frac{1}{\tau} \ . \tag{17}$$

Thus, besides the wave, a tube may be subject to a (nearly) constant flow q_{DC}, not being subject to wave attenuation. Since wave impedance Z is known, we may describe the zero-flow pressures $p_{\text{s,prox}}$ and $p_{\text{s,dist}}$ by adding a DC-component to the zero-flow wave pressures ($p_{\text{s,prox}}$ and $p_{\text{s,dist}}$, respectively) as calculated using Eq. 11:

$$\begin{aligned} \tilde{p}_{\text{s,prox}} &= p_{\text{s,prox}} - q_{\text{DC}} Z + \frac{\Delta p_{\text{DC}}}{2} \ , \\ \tilde{p}_{\text{s,dist}} &= p_{\text{s,dist}} + q_{\text{DC}} Z - \frac{\Delta p_{\text{DC}}}{2} \ . \end{aligned} \tag{18}$$

1.2 Arterio-venous impedance model

The terminal end of a tube is coupled to an arterio-venous impedance element (1). Such element resembles the classic three-element Windkessel (3WK), being composed of a resistor, compliance and characteristic impedance. Yet, important differences with respect

to the WK are that compliance is assumed pressure-dependent, and scaled by an estimate of the tissues' vessel bed length (1, 13), whereas wave impedance is assumed pressure-dependent:

$$C_x = l_{\text{AV}} \frac{dA}{dp_x} \text{ and } Z_{\text{wave},x} = \sqrt{\frac{\rho}{A} \frac{dp_x}{dA}} \,, \tag{19}$$

with x, the subscript for the arterial and venous contributions, i.e. $x = [\text{art}, \text{ven}]$. Such approach enables simulating large changes in hemodynamic load (e.g. exercise or hypertension) without requiring to change parameter values (1). The derivatives in the aforementioned equations were calculated at the distal node of a terminal tube, using the constitutive relation as given in Eq. 8. The parameter l_{AV} represents the characteristic length of a peripheral bed. We estimated the vessel bed length using the relation given by $l_{\text{AV}} = 6q_{\text{AV}}^{\frac{1}{3}}$, with q_{AV} the mean peripheral flow through any terminal tube. To obtain first-order approximations of l_{AV} among all peripheral beds, we utilized this relation in conjunction with flow distribution estimates. The peripheral resistance (R_{p}) was defined as a flow source, controlled by the instantaneous arterio-venous pressure difference (1):

$$R_{\text{p}} = \frac{p_{\text{art}} - p_{\text{ven}}}{q_{\text{AV}}} \,. \tag{20}$$

2 Benchmark comparison between TL and PWP model

For the benchmark comparison, we implemented a network of tubes describing the central arteries (i.e. the aorta, carotid artery, and vertebral artery), as well as the arteries of the left arm (Fig. 3). Geometrical and mechanical properties of all tubes were based on Reymond et al. (11). Vessel stiffness coefficient (k) for the aortic segments, vertebral artery and carotid artery was estimated by fitting the constitutive law (Eq. 8) to *in vitro* data from Hayashi et al. (5). For the radial, ulnar and interosseous arteries, stiffness was assumed equal to vertebral artery stiffness. For the subclavian–axillary–brachial arterial segment,

stiffness was taken as the mean of aortic and carotid artery stiffness. Flow fractions were based on previously published patient measurements with duplex ultrasound and phase-contrast magnetic resonance imaging (6).

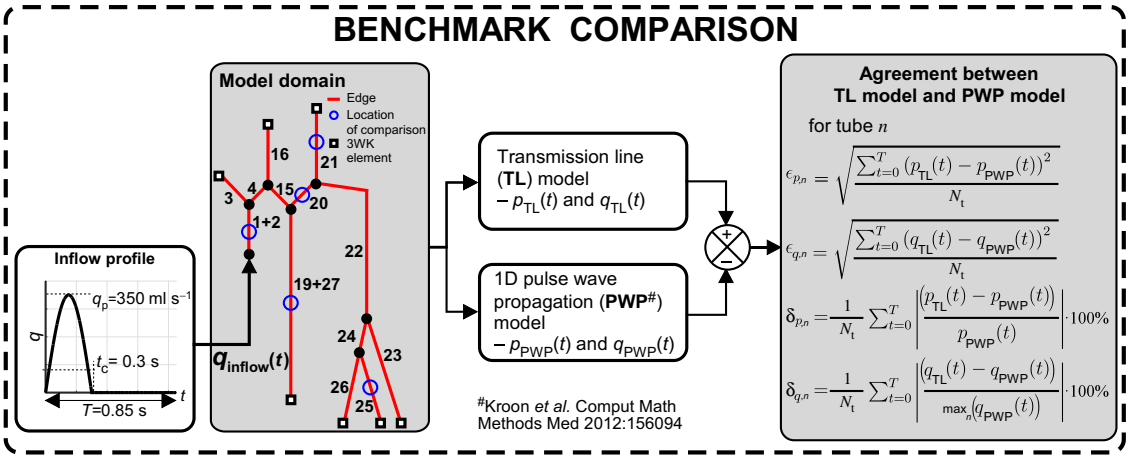

Figure 3: Benchmark comparison of the transmission line (TL) model with the previously validated 1D pulse wave propagation (PWP) model. We implemented a network of 13 tubes representing the large central arteries and the arteries of the left arm. A half-sinusoidal inflow profile (q_{inflow}) was prescribed to the ascending aorta. Boundary conditions; proximal inflow, termination of distal vessels, vessel geometry and material properties were kept the same for the TL model and PWP model. Agreement metrics chosen were root mean square errors ϵ_p and ϵ_q, as well as the relative errors δ_p and δ_q. Furthermore, N_t denotes the number of time points for which a comparison is made. A graphical comparison between pressure and flow waveforms is given for five tubes (blue circles). Tube segments: '1+2': ascending aorta, '3': brachiocephalic, '4': aortic arch A, '16': left common carotid, '15': aortic arch B, '19+27': thoracic aorta, '20': left subclavian, '21': left vertebral, '22': left subclavian + axillary + brachial, '23': left radial, '24': left ulnar A, '25': left interosseous, '26': left ulnar B.

For the benchmark comparison, we defined a half-sinusoidal inflow profile as a proximal inlet boundary condition $(q_{\text{inflow}}(t))$:

$$q_{\text{inflow}}(t) = \begin{cases} q_{\text{p}} \sin\left(\frac{\pi t}{t_{\text{c}}}\right) & \text{if } 0 \leq t \leq t_{\text{c}} \\ 0 & \text{if } t > t_{\text{c}} \ . \end{cases} \tag{21}$$

Distal tubes were terminated using the arterio-venous impedance model. For all simulations, time step (Δt) was kept at 0.5 ms, duty cycle (t_{c}) at 0.3 s, cardiac cycle duration (T) at 0.85 s, and peak flow rate (q_{p}) at 350 ml s^{-1}, resulting in a physiological cardiac out-

put. Boundary conditions were kept equal for the TL model and PWP model. Reference pressure (p_0) was kept at 105 mmHg, external pressure (p_{ext}) at 0 mmHg and outflow pressure at 4 mmHg. We chose an element size of 0.01 m. Convergence of the calculated hemodynamics was evaluated after each simulated cardiac cycle. Hereto, the calculated nodal pressures, $p(t)$, of the current cycle (i_{cyc}) were compared to those of the previous cycle ($i_{\text{cyc}} - 1$). An expression for the hemodynamics convergence norm (ϵ) is given as a relative root mean square:

$$\epsilon = \max_n \left(\sqrt{\frac{\sum_{t=0}^{T} \left(p_{n,i_{\text{cyc}}}^t - p_{n,i_{\text{cyc}}-1}^t \right)^2}{\sum_{t=0}^{T} \left(p_{n,i_{\text{cyc}}-1}^t \right)^2}} \right), \tag{22}$$

with n referring to the tube number. Throughout simulations, the hemodynamics convergence criterion was kept at 10^{-2}. Agreement between p and q waveforms, expressed by root mean square errors ϵ_p and ϵ_q, as well as relative errors δ_p and δ_q, was calculated for the center element of each tube (Fig. 3).

3 Results: Benchmark comparison between TL and PWP model

Validity of the TL model's numerical implementation was assessed by comparing pressure and flow waveforms generated by the TL model with those generated by the validated one-dimensional pulse wave propagation model of Kroon et al. (8). Agreement between pressure and flow waves of the TL model and PWP model for five tubes in the model domain is graphically depicted in Fig. 4. Hemodynamic convergence, indicated by $\epsilon < 10^{-2}$, of the TL model was achieved after four cycles and for the PWP model after six cycles. Root mean square errors for pressures and flows for all tubes are given in Table 1. In the ascending- (tube #1+2) and thoracic aorta (tube #19+27), agreement between pressure

and flow waveforms, expressed by relative errors was $[\delta_{p,1+2}, \delta_{p,19+27}] = [0.8, 0.8]$% and $[\delta_{q,1+2}, \delta_{q,19+27}] = [0.6, 2.3]$%, respectively. Furthermore, agreement between pressure and flow waveforms of the subclavian artery (tube #20) and vertebral artery (tube #21) was $[\delta_{p,20}, \delta_{p,21}] = [0.8, 1.5]$% and $[\delta_{q,20}, \delta_{q,21}] = [3.4, 2.9]$%, respectively. At the distally located interosseous artery, the difference between both models increased, expressed by $\delta_{p,25}$ equal to 2.9% and $\delta_{q,25}$ equal to 5.6%. Nevertheless, the shape of the pressure and flow waveforms as well as absolute systolic and diastolic pressure and flow values were highly similar (Fig 4).

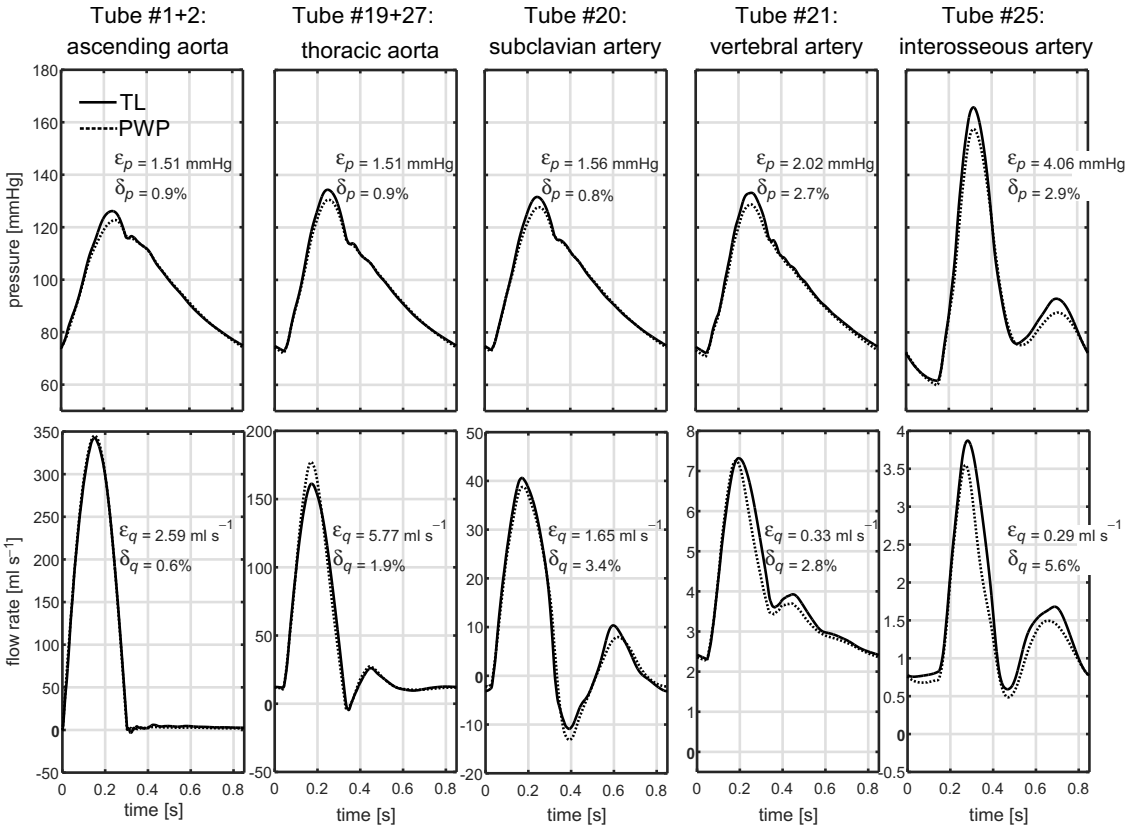

Figure 4: Results of the benchmark comparison. Pressure (p) and flow (q) waveforms generated by the transmission line (TL) model and 1D pulse wave propagation model (PWP) model are shown for various locations along the arterial domain. Agreement between p and q waveforms is expressed by root mean square errors ϵ_p and ϵ_q, as well as relative errors δ_p and δ_q.

Table 1: Benchmark comparison between pressure and flow waveforms of the transmission line (TL) model and pulse wave propagation (PWP) model. Root mean square errors (ϵ_p) for pressure and (ϵ_q) for flow, as well as relative errors (δ_p and δ_q) describe agreement between both models. Agreement was calculated for the element located at the center of the tube.

tube #	1+2	4	15	19+27	3	16	20	21	22	23	24	26	25
ϵ_p [mmHg]	1.51	1.54	2.26	1.58	1.58	1.51	1.56	2.02	2.87	4.02	3.74	4.08	4.06
ϵ_q [ml s^{-1}]	2.59	21.30	3.12	0.88	4.50	5.77	1.65	0.33	0.95	0.23	0.49	0.30	0.29
δ_p [%]	0.8	0.8	1.3	0.8	0.8	0.9	0.8	1.5	1.7	2.9	2.4	2.9	2.9
δ_q [%]	0.6	5.5	4.6	2.3	1.1	1.9	3.4	2.9	3.7	3.2	3.1	3.5	5.6

References

1. **Arts, T, Reesink, K, Kroon, W, Delhaas, T.** Simulation of adaptation of blood vessel geometry to flow and pressure: Implications for arterio-venous impedance. *Mechanics Research Communications* 42: 15–21, 2012.

2. **Bassez, S, Flaud, P, Chauveau, M.** Modeling of the deformation of flexible tubes using a single law: application to veins of the lower limb in man. *Journal of Biomechanical Engineering* 123: 58–65, 2001.

3. **Bessems, D, Rutten, M, Van De Vosse, F.** A wave propagation model of blood flow in large vessels using an approximate velocity profile function. *Journal of Fluid Mechanics* 580: 145–168, 2007.

4. **Boucher, R, Kitsios, E.** Simulation of fluid network dynamics by transmission line modelling. *Proceedings of the Institution of Mechanical Engineers, Part C: Journal of Mechanical Engineering Science* 200: 21–29, 1986.

5. **Hayashi, K, Handa, H, Nagasawa, S, Okumura, A, Moritake, K.** Stiffness and elastic behavior of human intracranial and extracranial arteries. *Journal of Biomechanics* 13: 175181–179184, 1980.

6. **Huberts, W, Bode, A, Kroon, W, Planken, R, Tordoir, J, Van de Vosse, F, Bosboom, E.** A pulse wave propagation model to support decision-making in vascular access planning in the clinic. *Medical Engineering & Physics* 34: 233–248, 2012.

7. **Hughes, TJ, Lubliner, J.** On the one-dimensional theory of blood flow in the larger vessels. *Mathematical Biosciences* 18: 161–170, 1973.

8. **Kroon, W, Huberts, W, Bosboom, M, van de Vosse, F.** A numerical method of reduced complexity for simulating vascular hemodynamics using coupled 0D lumped and 1D wave propagation models. *Computational and Mathematical Methods in Medicine*, 2012.

9. **Krus, P, Weddfelt, K, Palmberg, J-O.** Fast pipeline models for simulation of hydraulic systems. *Journal of Dynamic Systems, Measurement, and Control* 116: 132–136, 1994.

10. **Lumens, J, Delhaas, T, Kirn, B, Arts, T.** Three-wall segment (TriSeg) model describing mechanics and hemodynamics of ventricular interaction. *Annals of Biomedical Engineering* 37: 2234–2255, 2009.

11. **Reymond, P, Merenda, F, Perren, F, Rüfenacht, D, Stergiopulos, N.** Validation of a one-dimensional model of the systemic arterial tree. *American Journal of Physiology-Heart and Circulatory Physiology* 297: H208–H222, 2009.

12. **Walmsley, J, Arts, T, Derval, N, Bordachar, P, Cochet, H, Ploux, S, Prinzen, FW, Delhaas, T, Lumens, J.** Fast simulation of mechanical heterogeneity in the electrically asynchronous heart using the multipatch module. *PLoS Computational Biology* 11: e1004284, 2015.

13. **Wesseling, K, Jansen, J, Settels, J, Schreuder, J.** Computation of aortic flow from pressure in humans using a nonlinear, three-element model. *Journal of Applied Physiology* 74: 2566–2573, 1993.